Theoretical Study of the Insertion Reactions of Zr^+ into HF, HCl, H_2O, H_2S, NH_3, PH_3, CH_4, and SiH_4

Chaojie Wang,[†] Xin Xu,*[,†] Zhiji Cao,[†] Song Ye,[‡] and Qianer Zhang[†]

State Key Laboratory for Physical Chemistry of Solid Surfaces, Department of Chemistry, Institute for Physical Chemistry, Center for Theoretical Chemistry, Xiamen University, Xiamen 361005, People's Republic of China, and Department of Chemistry, Yunnan University, Kunming 650091, People's Republic of China

Received: January 16, 2003; In Final Form: June 17, 2003

The insertion reactions of transition metal cation doublet $Zr^+(^2D)$ into HF, HCl, H_2O, H_2S, NH_3, PH_3, CH_4, and SiH_4 have been studied by means of ab initio molecular orbital calculations incorporating electron correlation with the Møller−Plesset perturbation theory up to the second and the fourth orders and the hybrid density functional method, B3LYP. Three regions of the potential surface have been investigated, an ion−molecule complex, followed by a three-center, four-electron transition state, and then an insertion product. It is found that all insertion reactions are exothermic and all transition states are below the energy surfaces of the reactants. For the ion−molecule complexes, the binding energies of the same-row hydrides increase from right to left, with the exception of CH_4 and SiH_4, whose binding energies decline considerably; while to the same-group hydrides the ion−molecule complexes in the up row are more bound than those in the down row. The stability of the insertion product $H-Zr^+-RH_{n-1}$ decreases from right to left across the row and falls from up to down across the column. The reaction barrier follows the same trend; i.e., the more exothermic the insertion reaction is, the lower is the reaction barrier. All these observed trends could be understood by a combined effect of the electrostatic interaction and the covalent interaction.

1. Introduction

During the past decade, the insertion reactions of all sorts of atoms, ions, and free radicals into elementary molecules, which include prototypical R−H bonds (R = C, Si, N, P, O, and S), especially the C−H bond, have attracted much attention both experimentally and theoretically.[1−38]

Extensive experimental studies have been performed on reactions involving transition metal cations with hydrocarbons and some other molecules such as H_2 and NH_3, particularly by Armentrout and co-workers using a guided ion beam mass spectrometry.[1−8] It was believed that the reaction proceeds via (a) an ion−molecule complex, M^+-RH_n, then (b) a three-center, four-electron transition state, $H\cdots M^+\cdots RH_{n-1}$; and (c) an insertion product, $H-M^+-RH_{n-1}$.

$$\underset{\text{(a)}}{M^+-RH_n} \rightarrow \underset{\text{(b)}}{H\cdots M^+\cdots RH_{n-1}} \rightarrow \underset{\text{(c)}}{H-M^+-RH_{n-1}} \quad (1)$$

Reaction 1 is widely recognized as oxidative addition of M^+, as M^+ is formally oxidated by two units. Formation of the molecular complexes of M^+-NH_3 (M = Co, Ni, Cu) was evidenced experimentally, and the insertion complex $H-Co^+-NH_2$ was also detected.[5]

Based on the representative system of $M^+ + H_2$, three categories of the reactivity of M^+ appear to exist.[6] The deciding factors are the electron configuration and the spin state of the metal cation. (1) If *n*s and $(n-1)d_\sigma$ orbitals are empty, the systems react efficiently. (2) If either *n*s or $(n-1)d_\sigma$ is singly occupied, the systems can react efficiently as long as they have low spin. (3) High-spin systems with either *n*s or $(n-1)d_\sigma$ being singly occupied are unreactive. Reactions of the other $M^+ + RH_n$ systems are expected to parallel those for H−H bond activation, only the metal ion may not react diabatically. Reactions may undergo, according to adiabatic potential energy surfaces, mixing diabatic potential energy surfaces for states of the same spin but of different electron configurations.

Experimentally, the molecular complexes and the insertion products of some metal atoms (M = Li, Na, Mg, Al, Sc, Ti, V, Nb, Ta, and Cu) with RH_n type molecules including (HF, HCl, H_2O, H_2S, NH_3, and CH_4) have been reported.[9−19] Theoretically, Siegbahn and co-workers[20−26] have systematically investigated the insertion reactions between the entire sequence of the second-row neutral transition metal atoms and methane, ammonia, and water using methods including the electron correlation of all valence electrons. They have examined the lone-pair effects from the ligands. On one hand, the $Zr-CH_4$ molecular complex was found to be unbounded, and $Zr-NH_3$ and $Zr-H_2O$ were found to be bounded by 23.1 and 8.2 kcal/ mol, respectively.[21−23] This trend has been rationalized as CH_4 has no lone pair, and the lone pair in NH_3 is more diffuse than that in H_2O. On the other hand, the stability of the inserted product follows the trend that H−Zr−OH (BE = 66.3 kcal/mol) > $H-Zr-NH_2$ (49.6) > $H-Zr-CH_3$ (16.5).[21−23] This has been attributed to the fact that H_2O has two lone pairs, NH_3 has only one lone pair, and CH_4 has no lone pair. The activation barriers found are that $H\cdots Zr\cdots CH_3$ (24.6 kcal/mol) > $H\cdots Zr\cdots OH$ (5.9) > $H\cdots Zr\cdots NH_2$ (−1.0), where the shape of the lone pair, rather than the number of the lone pair, plays a crucial role.[21−23] The reaction between Zr^+ cation and CH_4 has also been investigated by Siegbahn et al.[20] As compared with the $Zr-CH_4$ neutral system, the molecular complex Zr^+-CH_4 is stabilized by 10.4 kcal/mol. The activation barrier has been

* Corresponding author. Fax: +86-592-218-3047. E-mail address: xinxu@xmu.edu.cn.
† Xiamen University.
‡ Yunnan University.

10.1021/jp034118o CCC: $25.00
Published on Web 08/05/2003

reduced from 24.6 to 16.2 kcal/mol. The final insertion product is, however, destabilized by 4.3 kcal/mol. Although the transition state and the insertion product were found to be in the low spin state, the molecular complex was located in the high spin state. All energetics were referred to the ground state of Zr^+ (^4F, d^2s^1). The spin conservation principle was not applied. Recently, some theoretical studies have appeared on the insertion reactions of the first-row transition metal cations into water, ammonia, and methane.[27−32]

A similar class of reactions, which have also been extensively studied by ab initio molecular theory, are the insertion reactions of the radicals CH, NH, SiH, and PH with HF, HCl, H_2O, H_2S, NH_3, and PH_3, due to their importance in combustion and in planetary atmospheric chemistry.[33−38]

Generally, it is very difficult to experimentally detect the molecular complexes, the insertion products, or the transition states, as they may all be short-lifetime species. Theory is therefore a potentially useful partner in an experiment in revealing the mechanism of a transition metal cation insertion into an RH_n molecule. RH_n with R = C, N, O, F and Si, P, S, Cl provides an ideal set of molecules for examining the periodic trends of the ligand effects on the insertion reaction. Systematic study with this whole set is, however, rare. Some of us have recently reported the Ti^+ insertion into R−H bonds in this set of hydrides.[29] Results of the Zr^+ insertion reactions are presented in this paper, aiming to establish some general rules on the basis of Armentrout's spin conservation concepts.[4]

2. Computational Method

Stationary points (minima and transition states) were located at the unrestricted Hartree−Fock (UHF) self-consistent field level. The UHF geometries for all reactants, molecular complexes, transition states, and insertion products were then used as the starting points for the full geometry optimizations performed at the unrestricted second-order Møller−Plesset perturbation (UMP2) level,[39] or the hybrid gradient-corrected exchange functional proposed by Becke, combined with the gradient-corrected correlation functional of Lee, Yang, and Parr (UB3LYP method[40−43]). Vibrational frequency calculations have been carried out at the MP2 or B3LYP level to characterize the stationary points obtained with the corresponding method. Single-point calculations were performed at the level of the unrestricted fourth-order Møller−Plesset perturbation[44] with single, double, triple, and quadruple substitutions (UMP4-(SDTQ) or MP4, for short) at the optimized MP2 geometries. In the case of $Zr^+ + H_2O$, the insertion reaction paths were explored at the UB3LYP level by determining the intrinsic reaction coordinate (IRC).[45,46]

In this work, a relativistic effective core potential (RECP) was employed to replace the 1s to 3d core electrons of zirconium, while the electrons arising from the outer 4s4p4d5s5p shells were treated explicitly.[47] The Gaussian-type orbital (GTO) basis set for the RECP of Zr includes 5s, 6p, and 3d primitive functions contracted to [3s3p2d]. This basis set is referred to as Lanl2dz in the Gaussian suite of programs.[48] The standard 6-31G** basis sets for F, Cl, O, S, N, P, C, Si, and H atoms were used.[49] These 6-31G**(Lanl2dz) basis sets were used for doing geometric optimizations and calculations of the vibrational frequencies. To improve the accuracy of the energetic results, single point calculations at the MP2, MP4, and B3LYP levels have been performed with Zr^+ Lanl2dz basis set being augmented with an f polarization function, denoted as 6-31G**-(Lanl2dz+f).[50]

The potential energy surfaces explored here are for the low multiplicity of the doublet, $Zr^+(a^2D)$. The energetics data reported are reaction enthalpy changes at 0 K at the MP4(SDTQ) or B3LYP level with 6-31G**(Lanl2dz+f). Unscaled zero-point energies obtained with MP2/6-31G**(Lanl2dz) were used to correct the MP4/6-31G**(Lanl2dz+f) energies; while those from B3LYP/6-31G**(Lanl2dz) were used for the B3LYP/6-31G**(Lanl2dz+f) energy corrections. Detailed energetic information can be found in the Supporting Information, where a table summarizing the calculated relative energies of Zr^+ (a^4F, b^4F, a^2D, a^2F, a^2G) is also presented. Spin projection technique has be applied to all the energies reported here, although there is discussion on the validity of using the projected DFT methods.[51−53]

For calculation of the binding energy of an ion−molecule complex, the basis set superposition error (BSSE) may be important. We calculated the BSSE corrections with the full counterpoise procedure.[54]

$$\Delta E(\mathrm{BSSE,A-D}) = E(\mathrm{A})_{\mathrm{A}} - E(\mathrm{A})_{\mathrm{A-D}} + E(\mathrm{D})_{\mathrm{D}} - E(\mathrm{D})_{\mathrm{A-D}} \quad (2)$$

where $E(A)_{A-D}$ and $E(A)_A$ represent the energy of A calculated using its geometry within the complex and the basis functions of A + D in the former and those of A alone in the latter. The BSSE results are summarized in the Supporting Information.

All calculations were done with the Gaussian 98 program.[48]

3. Results and Discussion

3.1. Ion−Molecule Precursor Complex Zr^+−RH_n. The optimized geometries of the ion−molecule precursor complexes (*n*a or *n*a′, *n* = 1−8) are depicted in Figures 1 and 2. The trends of the binding energies at PMP4 and PB3LYP levels shown in Figure 3 can be described in the following way. First, the binding energy of the same-row hydride increases from right to left, with the exception of CH_4 or SiH_4, whose binding energy declines considerably. Second, to the same-group hydrides the ion−molecule complexes in the up row are more bound than those in the down row, with the exception of CH_4 and SiH_4, where the reverse trend is observed.

Two kinds of interactions contribute to the stabilization of the ion−molecular complexes. One is the electrostatic interaction between the transition metal cation Zr^+ and the dipole (or induced dipole) moment of RH_n. The other is the orbital interaction between the lone pairs of RH_n and the empty orbitals of Zr^+. The subtle balance between the electrostatic effect and the covalent effect determines the relative stability of the molecular complexes Zr^+−RH_n of varying R.

From an electrostatic point of view, the leading terms of the binding energy can be written as

$$\mathrm{BE} = \mu q \cos(\theta)/r^2 + \alpha q^2/2r^4 \quad (3)$$

Here μ and α are the dipole moment and the polarizability of RH_n, respectively, q is the elementary charge on the ion, r is the distance between the ion and RH_n, and θ is the angle between r and μ. Thus, when a cation is near a dipolar molecule, the maximum attraction will occur when the dipole points away from the ion (θ = 0 or 180°). And a higher permanent dipole moment μ or a larger polarizability α or a shorter interaction distance r will lead to a larger stabilization of Zr^+−RH_n.

Table 1 summarizes the calculated μ and α at the B3LYP level. The corresponding experimental values are included in parentheses for comparison. It is well-known that the dipole moment and the polarizability are hard to calculate. It is therefore not surprising to see that μ is overestimated and α is underestimated by theory. It is generally true that the dipole

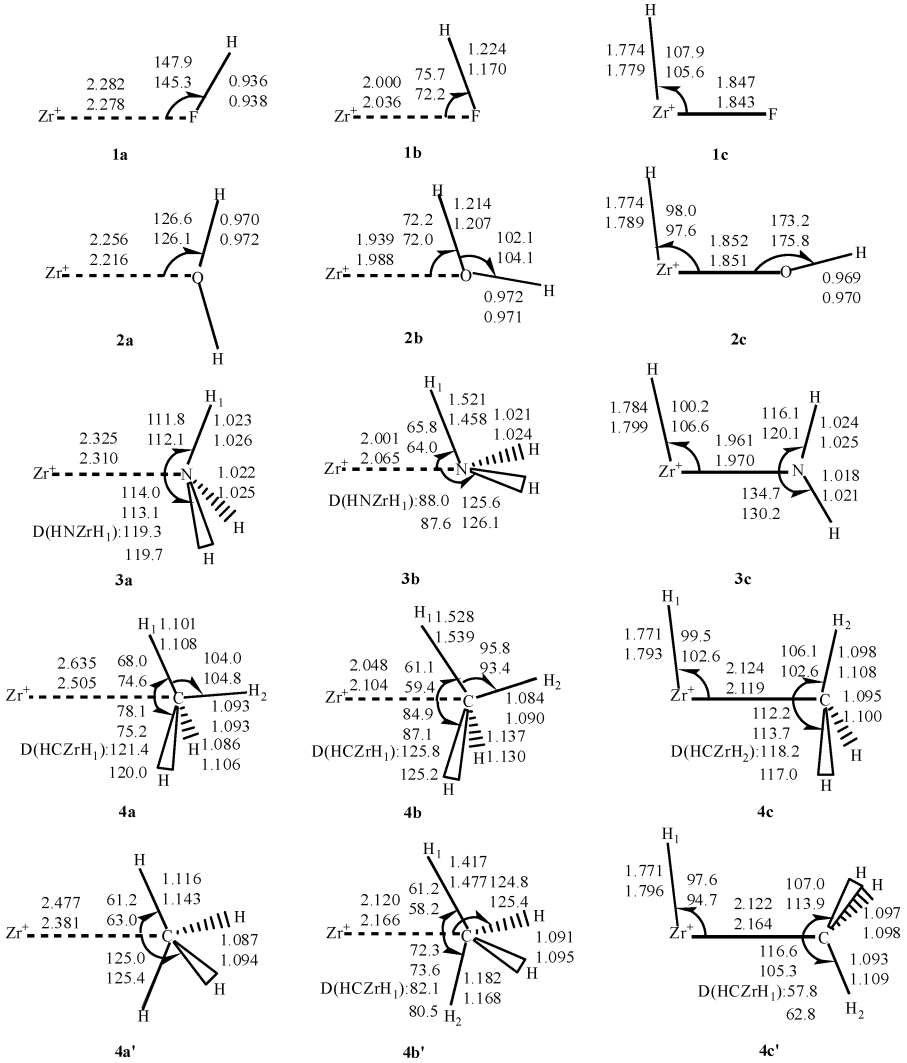

Figure 1. Optimized geometries (bond lengths, Å; bond angles, deg) for the ion−molecule precursor complexes (*n*a or *n*a′, $n = 1-4$), the transition states (*n*b or *n*b′), and the insertion products (*n*c or *n*c′) of Zr^+ with HF, H_2O, NH_3, and CH_4 molecules. The parameters were optimized at MP2/6-31G**(Lanl2dz) and B3LYP/6-31G**(Lanl2dz) levels from up to down.

moment of the second-row RH_n is smaller than that of the first-row RH_n; while the polarizability of the second-row RH_n is larger than that of the first-row RH_n, which is however compensated by an increase of the Zr^+-RH_n distance r from up row to down row. On the basis of eq 3 it is clear that the electrostatic stabilization is less in the second-row hydride-ion complex Zr^+-RH_n than that in the corresponding first-row hydride-ion complex. As R crossing the row from right (F or Cl) to left (C or Si), the electrostatic stabilization from the ion−dipole interaction gradually decreases, and there is only ion-induced dipole interaction in Zr^+-CH_4 or Zr^+-SiH_4. The observed increase of the stability of Zr^+-RH_n from right (F or Cl) to left (N or P) should be correlated with the increased ion-induced dipole interaction from an electrostatic point of view.

On the basis of eq 3, the electrostatic contribution to the total binding energy of the molecular complex Zr^+-RH_n could be estimated (e.g. 23.3, 35.4, 32.8, and 9.5 kcal/mol for RH_n = HF, H_2O, NH_3, and CH_4). Suppose that all the other contributions from charge transfer and exchange energy cost, etc., could be denoted as the covalent contribution, based on the PB3LYP/6-31G**(Lanl2dz+f) results, in this series would be 5.4, 9.2, 27.3, and 7.5 kcal/mol as R varies from F to C. It is seen that the covalent contribution is less important than the electrostatic contribution in the molecular complexes of Zr^+-HF and Zr^+-H_2O, while for Zr^+-NH_3 and Zr^+-CH_4 the covalent contribution is comparable to the electrostatic contribution. Even though there is no lone pair on CH_4, there exists a large covalent contribution. Mulliken population analysis shows that upon forming the molecular complex Zr^+-CH_4, CH_4 is positively charged by ∼0.21 au, with Zr^+ being reduced. Thus, there should be a considerable amount of charge transfer from the bonding orbitals of C−H in CH_4 to the empty orbital of Zr^+.

All the Zr^+-R bond distances optimized at the MP2 level are longer than those obtained at the B3LYP level. As compared to that in the free ligand RH_n, there is only slight elongation of the corresponding R−H bond upon forming a Zr^+-RH_n complex. It is interesting to see that the Zr^+-R-H angle in an ion−molecule complex of the first-row hydride is generally bigger than that of the second-row hydride of the same group. This would be a way to reduce the electrostatic repulsion between the positive charge on Zr^+ and the positive charge on H in a hydride or it would increase the electrostatic interaction between Zr^+ and the negatively charged H in the PH_3 or SiH_4 molecule. Although a linear structure will maximize the ion−dipole interaction, both Zr^+-FH (**1a**) and Zr^+-ClH (**5a**) are found to adopt a bent structure. This should be attributed to the electron donation from a lone pair orbital of the halogen hydride to the empty d orbital of Zr^+. On the other hand, the geometric structure of Zr^+-RH_2 (R = O or S) provides an example in which the electrostatic interaction outweighs the covalent

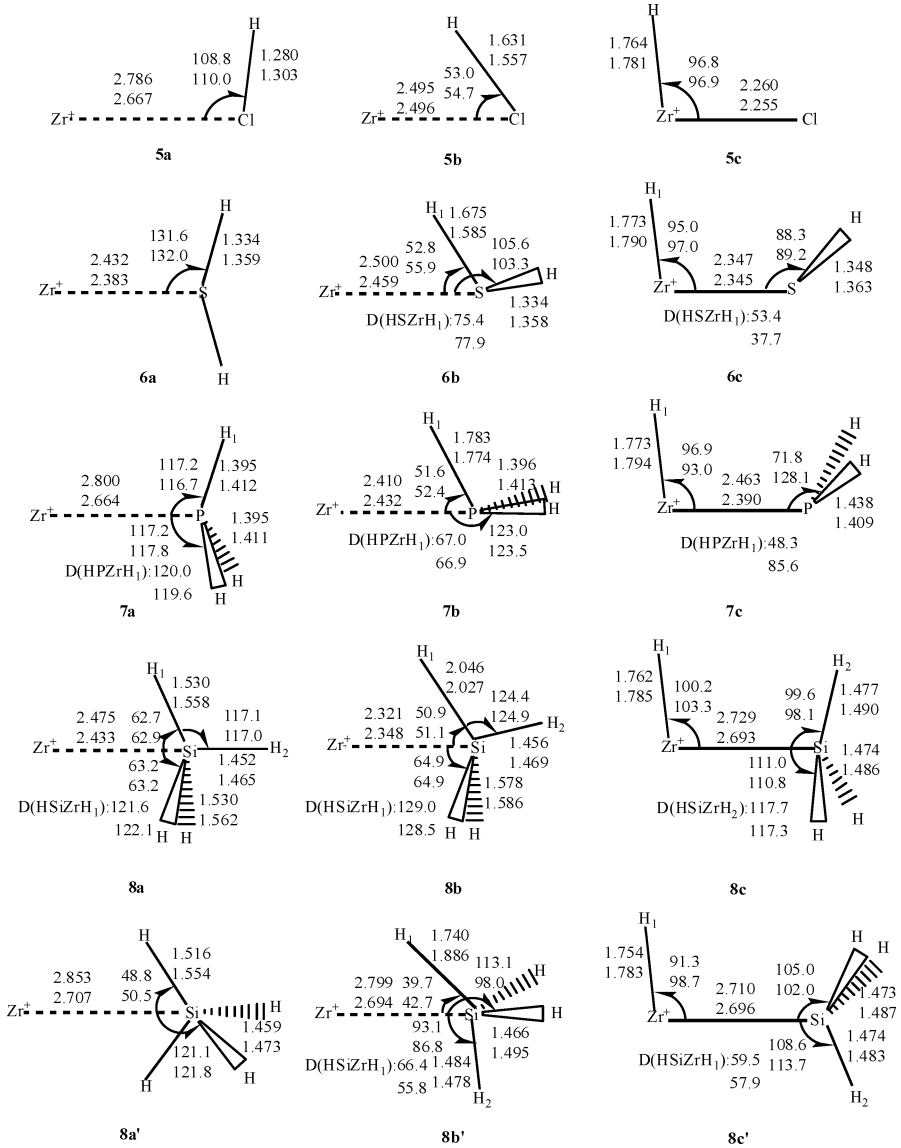

Figure 2. Optimized geometries (bond lengths, Å; bond angles, deg) for the ion−molecule precursor complexes (*n*a or *n*a′, $n = 5-8$), the transition states (*n*b or *n*b′), and the insertion products (*n*c or *n*c′) of Zr^+ with HCl, H_2S, PH_3, and SiH_4 molecules. The parameters were optimized at MP2/6-31G**(Lanl2dz) and B3LYP/6-31G**(Lanl2dz) levels from up to down.

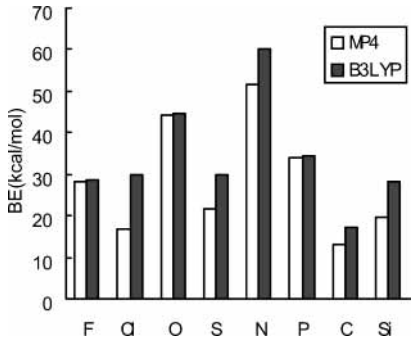

Figure 3. Relative stability of ion−molecular complex Zr^+-RH_n, calculated at the PMP4 and PB3LYP levels. $BE(Zr^+-RH_n) = E_{tot.}(Zr^+) + E_{tot.}(RH_n) - E_{tot.}(Zr^+-RH_n)$.

interaction. Instead of adopting a nonplanar C_s symmetry, binding along the direction of one lone pair of RH_2 to maximize the covalent bonding, Zr^+ binds to RH_2 in the direction of the dipole moment of RH_2, forming a planar Zr^+-RH_2 complex with C_{2v} symmetry. Zr^+-NH_3 (**3a**) and Zr^+-PH_3 (**7a**) both have C_s symmetry due to a Jahn-Teller effect. Zr^+-CH_4 or Zr^+-SiH_4 has isomers **4a** and **4a′** or **8a** and **8a′**. Molecular complexes **4a** and **8a** were found to have a slightly tilted η^3 coordination mode with C_s symmetry, while **4a′** and **8a′** are η^2 coordinated with C_{2v} symmetry. The Zr^+-C bond distances in **4a** and **4a′** are 2.635 and 2.477 Å at the MP2 level or 2.505 and 2.381 Å at the B3LYP level. It is interesting to see that Zr^+-Si bond is shorter than the Zr^+-C bond in **4a** and **8a**. This has to be attributed to the fact that SiH_4 is more polarizable than CH_4 so that the covalent effect is more dominant in Zr^+-SiH_4 than it is in Zr^+-CH_4.

3.2. Insertion Products $H-Zr^+-RH_{n-1}$. As it is shown in Figure 4, to the same-row hydrides, the stability of the insertion products decreases from right to left; while to the same-group hydrides, the stability falls from up to down. This might be correlated with the facts that the number of lone pairs decreases along the row from right to left and the electronegativity of the center R atom falls gradually from up to down. The reaction enthalpies of Zr^+ with the first-row hydrides from HF to CH_4 are −96.8, −93.8, −74.0, and −34.2 kcal/mol at the PMP4 level and −91.2, −88.9, −75.5, and −37.9 kcal/mol at the PB3LYP level, while those with the second-row hydrides from HCl to SiH_4 are −70.6, −62.3, −44.4, and −25.0 kcal/mol at the PMP4 level and −73.6, −65.9, −48.9, and −31.0 kcal/mol at the

TABLE 1: Geometric Parameters (H−R Bond Lengths, Å; ∠HRH Bond Angles, deg), Dipole Moment (μ, D), Polarizability (α, Å^3), and Mulliken Charges for the Free Ligands RH_n at the B3LYP Level[a]

species	H−R	∠HRH	μ	α	Q(R)	Q(H)
HF	0.925 (0.917)		1.83 (1.91)	0.52	−0.36	0.36
H_2O	0.965 (0.958)	103.7 (104.5)	2.04 (1.85)	0.96 (1.48)	−0.60	0.30
NH_3	1.018 (1.015)	105.8 (106.8)	1.84 (1.47)	1.53 (2.21)	−0.72	0.24
CH_4	1.092 (1.091)	109.5 (109.5)	0.0 (0.0)	2.25 (2.56)	−0.48	0.12
HCl	1.286 (1.274)		1.43 (1.08)	1.70 (2.63)	−0.19	0.19
H_2S	1.348 (1.334)	92.7 (92.3)	1.40 (1.10)	3.04 (3.78)	−0.16	0.08
PH_3	1.424 (1.421)	93.5 (93.5)	0.96	4.35	0.01	−0.00
SiH_4	1.485 (1.477)	109.5 (109.5)	0.0 (0.0)	4.40 (5.44)	0.32	−0.08

[a] Experimental values are included in parentheses for comparison. All experimental values are cited from: *CRC Handbook of Chemistry and Physics*, 66th ed.; Weast, R. C., Ed.; CRC Press: Boca Raton, FL, 1985.

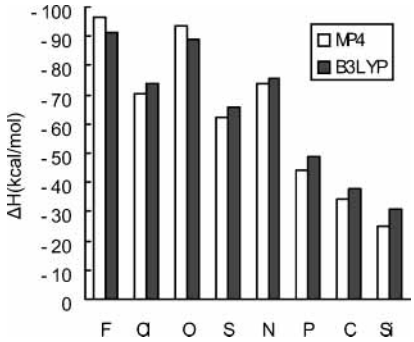

Figure 4. Relative energies for the insertion product $H-Zr^+-RH_{n-1}$. $\Delta H(H-Zr^+-RH_{n-1}) = E_{tot.}(H-Zr^+-RH_{n-1}) - E_{tot.}(Zr^+) - E_{tot.}(RH_n)$ at PMP4 and PB3LYP levels. Negative values indicate that insertion reactions are exothermic.

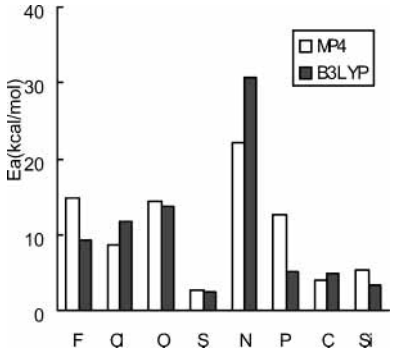

Figure 5. Barrier heights for Zr^+ insertions into R−H bonds in RH_n (R = F, Cl, O, S, N, P, C, and Si) calculated at PMP4 and PB3LYP levels. $E_a = E_{tot.}(H\cdots Zr^+\cdots RH_{n-1}) - E_{tot.}(Zr^+-RH_n)$.

PB3LYP level. All the insertion reactions of the transition metal cation Zr^+ into these eight kinds of hydrides are exothermic.

To form an insertion product of $H-Zr^+-RH_{n-1}$, it is necessary to break an $H-RH_{n-1}$ bond and to make an $H-Zr^+$ bond as well as a Zr^+-RH_{n-1} bond. This process could be best understood by the Born−Harber cycle.

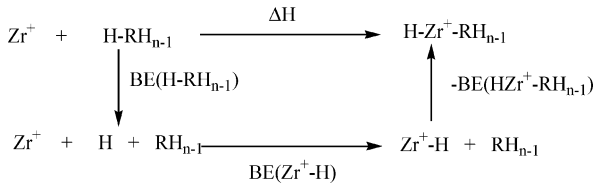

Assuming that the $H-Zr^+$ bond energy and the exchange energy loss upon bonding are similar in all $H-Zr^+-RH_{n-1}$, the relative stability of $H-Zr^+-RH_{n-1}$ could be rationalized by the energy difference between an $H-RH_{n-1}$ and a Zr^+-RH_{n-1} bond; i.e., $\Delta BE = BE(Zr^+-RH_{n-1}) - BE(H-RH_{n-1})$. Table 2 lists the B3LYP bond energies of $H-RH_n$. The calculated values agree well with the available experimental data shown in parentheses. Table 2 also summarizes the B3LYP bond energies of the Zr^+-RH_{n-1} bond and ΔBEs. As is clear from Table 2, the Zr^+-F bond is 20 kcal/mol stronger than the H−F bond; while the Zr^+-SiH_3 bond is 36.2 weaker than $H-SiH_3$. Therefore among these series, the insertion product $H-Zr^+-F$ (**1c**) is the most stable species of all, while the insertion product $H-Zr^+-SiH_3$ (**8c**) is the least stable. As a matter of fact, the periodic change of ΔBE nicely explains the observed trend that the stability of the insertion products decreases from right to left across the row and falls from up to down across the column.

The insertion products $H-Zr^+-RH_{n-1}$ might decompose into $H-Zr^+$ or Zr^+-RH_{n-1} fragments. Our calculations show the decomposition is endothermic and therefore unfavorable in energy. Further dehydrogenation of an insertion product to make H_2 plus Zr^+-RH_{n-2} is found to be feasible. In fact, for Zr^+ + H_2O and Zr^+ + NH_3 systems, formations of H_2 + ZrO^+ and H_2 + $ZrNH^+$ are predicted to be exothermic by −91.7 and −52.0 kcal/mol at the MP4 level, respectively.

The Zr^+-H bond distance in $H-Zr^+-RH_{n-1}$ is nearly equal to the value of $H-Zr^+$ ion (1.79 Å at the MP2 level or 1.80 Å at the B3LYP level). The $H-Zr^+-R$ angle is around 100°; $H-O-Zr^+$ angle in 2c is around 180°. The linear $H-O-Zr^+$ structure maximizes the $O\rightarrow Zr^+$ dative π bond. Both planar **3c** and **7c** and out-of-planar **3c′** and **7c′** insertion products are found to exist in Zr^+ + NH_3 and Zr^+ + PH_3 systems.

3.3. Transition State $H\cdots Zr^+\cdots RH_{n-1}$. The transition state (TS, *n*b or *n*b′) connects an ion−molecule complex to the corresponding insertion product. It corresponds to the migration of one H atom from the center atom R in RH_n to the transition metal cation Zr^+. All TS′ are true transition states with the exception of **8b′**, which possesses two imaginary frequencies. Figure 5 shows that the barrier heights, with respect to the molecular complexes Zr^+-RH_n, for the same-group hydrides fall from up to down. The values obtained by the B3LYP method parallel to those of MP4.

The R−H bond dissociation energies in the first-row hydrides are all higher than those in the second-row RH_n. This should lead to cleavage of one R−H bond in the first-row hydrides being more difficult. As a matter of fact, there is a partial breaking of the R−H bond and a partial formation of Zr^+-R and Zr^+-H bonds in the TS; the observed periodic trend of the barrier heights can be correlated with ΔBE. That is, the barrier heights increase from right (HF) to left (NH_3) with a drop at CH_4. For the second-row hydrides of HCl to SiH_4, however, the trend is not so obvious. It is worthy to notice that all TS are below the reactants Zr^+ + RH_n in the overall energy surface.

All TSs have C_s symmetry. The Zr^+-R bond distance is generally shorter than that in the corresponding ion−molecule complex; e.g., the Zr^+-O bond length is 2.256 Å in **2a** but 1.939Å in **2b** at the MP2 level. The activated R−H bond is much elongated as compared to that in the free hydride. For

TABLE 2: Bond Energies BE(H−RH$_{n-1}$) and BE(Zr$^+$−RH$_{n-1}$) and Bond Energy Difference ΔBE = BE(Zr$^+$−RH$_{n-1}$) − BE(H−RH$_{n-1}$) at B3LYP[a]

	F	O	N	C	Cl	S	P	Si
BE(H−RH$_{n-1}$)	132.8 (136.2)	119.8 (119)	112.0 (108)	113.5 (105.0)	103.1 (103.1)	92.9 (90.5)	86.0	95.4 (92.0)
BE(Zr$^+$−RH$_{n-1}$)	153.2	136.6	113.4	78.8	109.9	90.6	68.1	59.2
ΔBE	20.4	16.8	1.4	−34.7	6.8	−2.3	−17.9	−36.2

[a] Experimental values are included in parentheses for comparison. All experimental values are cited from: *CRC Handbook of Chemistry and Physics*, 66th ed.; Weast, R. C., Ed.; CRC Press: Boca Raton, FL, 1985.

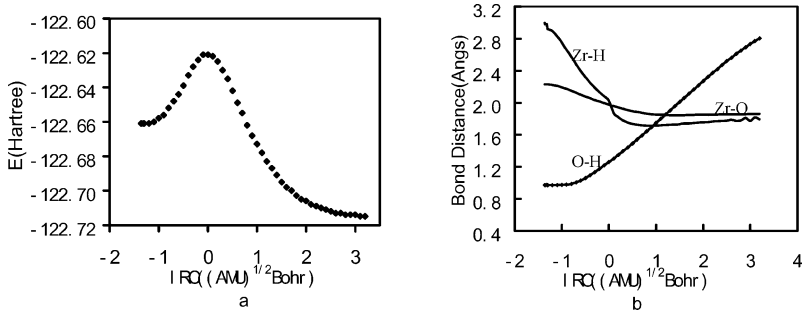

Figure 6. Changes of total energy (a) and bond distances (b) along the insertion reaction path in the Zr$^+$ + H$_2$O system.

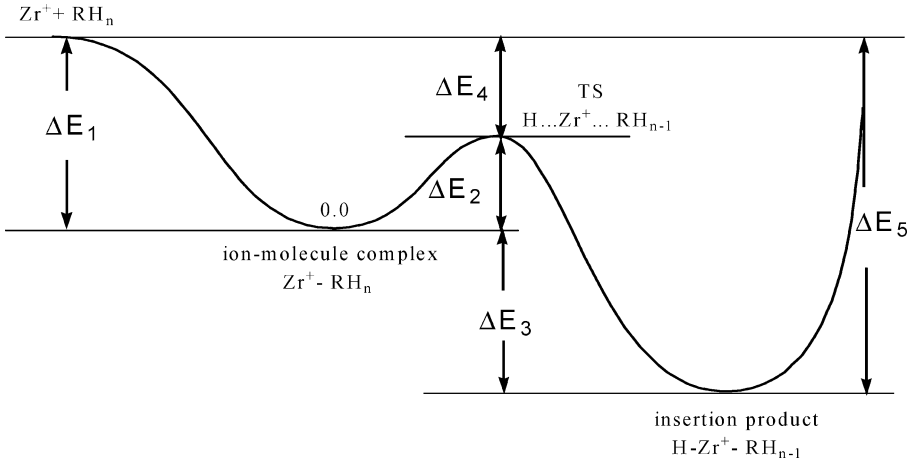

Figure 7. Energy profile for Zr$^+$ insertion into H−RH$_{n-1}$ via ion−molecule complex M$^+$−RH$_n$, transition state H···M$^+$···RH$_{n-1}$ to insertion product H−M$^+$−RH$_{n-1}$.

TABLE 3: Relative Energies (kcal/mol) for the Insertion Reaction Zr$^+$ + RH$_n$ → Ion−Molecule Complex Zr$^+$−RH$_n$ → Transition State H···Zr$^+$···RH$_{n-1}$ → Insertion Product H−Zr$^+$−RH$_{n-1}$ at PMP2, (PMP4), and [PB3LYP], where $\Delta E_1 = E_{tot.}$(Zr$^+$) + $E_{tot.}$(RH$_n$) − $E_{tot.}$(Zr$^+$−RH$_n$); $\Delta E_2 = E_{tot.}$(H···Zr$^+$···RH$_{n-1}$) − $E_{tot.}$(Zr$^+$−RH$_n$); $\Delta E_3 = E_{tot.}$(H−Zr$^+$−RH$_{n-1}$) − $E_{tot.}$(Zr$^+$−RH$_n$); $\Delta E_4 = \Delta E_1 - \Delta E_2$; and $\Delta E_5 = \Delta E_1 - \Delta E_3$

	F	O	N	C	Cl	S	P	Si
ΔE_1	28.0	44.0	51.8	12.9	16.2	21.0	33.9	24.6
	(28.2)	(44.2)	(51.6)	(13.3)	(16.6)	(21.9)	(33.9)	(25.8)
	[28.7]	[44.6]	[60.1]	[17.0]	[23.8]	[29.7]	[34.3]	[28.4]
ΔE_2	16.4	15.2	23.1	3.5	9.3	2.9	14.2	5.5
	(14.9)	(14.3)	(22.1)	(3.9)	(8.7)	(2.7)	(12.6)	(5.3)
	[9.3]	[13.8]	[30.7]	[4.8]	[11.7]	[2.5]	[5.1]	[3.3]
ΔE_3	−65.1	−47.7	−22.0	−21.2	−52.1	−39.4	−8.8	−5.5
	(−68.6)	(−49.6)	(−22.4)	(−20.9)	(−54.0)	(−40.4)	(−10.5)	(−5.2)
	[−62.5]	[−44.3]	[−15.4]	[−20.9]	[−49.8]	[−36.2]	[−14.6]	[−2.6]
ΔE_4	11.6	28.8	28.7	9.4	6.9	18.1	19.7	19.1
	(13.3)	(29.9)	(29.5)	(9.4)	(7.9)	(19.2)	(21.3)	(20.5)
	[19.4]	[30.6]	[29.4]	[11.2]	[12.1]	[27.2]	[29.2]	[25.1]
ΔE_5	93.1	91.7	73.8	34.1	68.3	60.4	42.7	30.1
	(96.8)	(93.8)	(74.0)	(34.2)	(70.6)	(62.3)	(44.4)	(31.0)
	[91.2]	[88.9]	[75.5]	[37.9]	[73.6]	[65.9]	[49.2]	[31.0]

example, the O−H bond distance in H$_2$O is 0.961 Å but 1.214 Å in **3b** at the MP2 level.

Representative IRC calculation on Zr$^+$ + H$_2$O system has been performed at the UB3LYP level. The total energy change along the IRC path is shown in Figure 6a. The variations of Zr−O, O−H, and Zr−H bond distances along the IRC path are shown in Figure 6b. From point −1.5 to −0.8, there is only a slight increase of the total energy, accompanied by a small decrease in the Zr$^+$−H and Zr$^+$−O bond distances. The O−H bond is hardly perturbed, and the molecular complex Zr$^+$−H$_2$O is only slightly activated in this region. As the reaction coordinate passes from point −0.8 to point 0 (TS), the total energy increases sharply and reaches its maximum. In this region, the Zr$^+$−H distance decreases dramatically. As the Zr$^+$−H bond starts forming, the O−H bond begins decomposing. The region from point 0 to point +1.5 could be denoted as

the H insertion region, where the Zr^+-H bond is formed. We believe that all M^+ insertion into RH_n hydrides to make $H-M^+-RH_{n-1}$ should bear certain resemblance with the Zr^+-H_2O system shown here.

4. Concluding Remarks

In the present work, the insertion reaction mechanism of the transition metal cation doublet Zr^+ with eight kinds of ordinary hydrides of the first-row HF, H_2O, NH_3, and CH_4 molecules and the second-row HCl, H_2S, PH_3, and SiH_4 molecules, has been studied by ab initio method and density functional theory. The reaction profile is schematically presented in Figure 7, and the reaction energetics is summarized in Table 3. Taking the reactants $Zr^+ + RH_n$ as a reference, all insertion reactions are exothermic and all transition states are below the energy surfaces of the reactants.

There exist stable ion−molecular complexes. The relative stability of the ion−molecular complexes Zr^+-RH_n depends on the subtle balance between the electrostatic effect and the covalent effect. It is found that the binding energy of the same-row hydride increases from right to left, with the exception of CH_4 and SiH_4, whose binding energies decline considerably; while to the same-group hydrides the ion−molecule complexes in the up row are more bound than those in the down row.

If the insertion reaction follows a trapping-mediated mechanism, it would be appropriate to take the ion−molecule complex Zr^+-RH_n as a reference state for the insertion reaction. As is seen from Table 3, the stability of the insertion products $H-Zr^+-RH_{n-1}$ decreases from right to left across the row and falls from up to down across the column. The reaction barrier follows the same trend; i.e., the more exothermic the insertion reaction is, the lower is the reaction barrier. All these trends can be rationalized by the relative bond strength between an $H-RH_{n-1}$ and a Zr^+-RH_{n-1} bond.

As compared to the previous studies,[27,29] it is seen that the Zr^+ chemistry parallels the Ti^+ chemistry. However, since the radius of Zr^+ is larger than that of Ti^+, the $r(Zr^+\cdots RH_n)$ distance is longer than $r(Ti^+\cdots RH_n)$ in the molecular complex such that the electrostatic stabilization in Ti^+-RH_n should be larger than that in the corresponding Zr^+-RH_n. As Ti^+ is more reducible than Zr^+, hence, the covalent bonding contribution ($M^+\leftarrow L$) should be larger in Ti^+-RH_n. Therefore, both electrostatic and covalent contributions lead to a higher binding energies in the molecular complex of Ti^+-RH_n as compared to that in the corresponding Zr^+-RH_n. On the other hand, since Zr^+ is easier to oxidize than Ti^+, we see that the insertion barrier is lower in $H\cdots Zr^+\cdots RH_{n-1}$ and the insertion reaction is more exothermic in $H-Zr^+-RH_{n-1}$ than in the corresponding Ti^+ chemistry.

Acknowledgment. This work is supported by the Natural Science Foundation of China (Grants 20021002 and 20973031) and TRAPOYT from the Ministry of Education of China.

Supporting Information Available: Tables of detailed energetic information. This material is available free of charge via the Internet at http://pubs.acs.org.

References and Notes

(1) Sunderlin, L. S.; Armentrout, P. B. *J. Phys. Chem.* **1988**, *92*, 1209.
(2) Clemmer, D. E.; Armentrout, P. B. *J. Am. Chem. Soc.* **1989**, *111*, 8280.
(3) Sunderlin, L. S.; Armentrout, P. B. *J. Phys. Chem.* **1990**, *94*, 3008.
(4) Armentrout, P. B. *Annu. Rev. Phys. Chem.* **1990**, *41*, 313.
(5) Clemmer, D. E.; Armentrout, P. B. *J. Phys. Chem.* **1991**, *95*, 3084.
(6) Armentrout, P. B. In *Selective Hydrocarbon Activation Principles and Progress*; Davis, J. A., Watson, P. L., Greenberg, A., Liebman, J. F., Eds.; VCH Publishers: New York, 1990; p 467.
(7) Chen, Y. M.; Armentrout, P. B. *J. Phys. Chem.* **1995**, *99*, 10775.
(8) Michael, R. S.; Chen, Y. M.; Elkind, J. L.; Armentrout, P. B. *J. Phys. Chem.* **1996**, *100*, 54.
(9) Shpiro, M.; Zeiri, Y. *J. Chem. Phys.* **1979**, *70*, 5264.
(10) Kauffman, J. W.; Hange, R. H. *J. Phys. Chem.* **1985**, *89*, 3547.
(11) Parnis, J. M.; Ozin Getffrey, A. *J. Am. Chem. Soc.* **1985**, *107*, 8169.
(12) Parnis, J. M.; Ozin Getffrey, A. *J. Am. Chem. Soc.* **1986**, *108*, 1699.
(13) Howard, J. A.; Joly, H. A.; Edwards, P. P.; Singer, R. J.; Longan, D. E. *J. Am. Chem. Soc*. **1992**, *114*, 474.
(14) Honma, H.; Nakamura, M.; Clemmer, D. E.; Koyano, I. *J. Phys. Chem.* **1994**, *98*, 13286.
(15) Senda, K.; Matsui, R.; Honma, K. *J. Phys. Chem.* **1995**, *99*, 13992.
(16) Belyung, D. P.; Hranisavljevic, J.; Kashireninov, O. E.; Santana, G. M.; Fontijn A. *J. Phys. Chem.* **1996**, *100*, 17835.
(17) Zhou, M. F.; Dong, J.; Zhang, L.; Qin, Q. *J. Am. Chem. Soc*. **2001**, *123*, 135.
(18) Dong, J.; Zhang, L.; Zhou, M. F. *J. Phys. Chem. A* **2000**, *104*, 8882.
(19) Honma, H.; Nakamura, M.; Clemmer, D. E.; Koyano, I. *J. Phys. Chem.* **1994**, *98*, 13286.
(20) Blomberg, M. R. A.; Siegbehn, P. E. M.; Svensson, M. *J. Phys. Chem.* **1994**, *98*, 2062.
(21) Blomberg, M. R. A.; Siegbehn, P. E. M.; Svensson, M. *Inorg. Chem.* **1993**, *32*, 4218.
(22) Blomberg, M. R. A.; Siegbahn, P. E. M.; Svensson, M. *J. Am. Chem. Soc.* **1992**, *114*, 6095.
(23) Siegbahn, P. E. M.; Blomberg, M. R. A.; Svensson, M. *J. Phys. Chem.* **1993**, *97*, 2564.
(24) Jensen, V. R.; Siegbahn, P. E. M. *Chem. Phys. Lett.* **1993**, *212*, 353.
(25) Siegbahn, P. E. M.; Blomberg, M. R. A.; Svensson, M. *J. Am. Chem. Soc.* **1993**, *115*, 1952.
(26) Siegbahn, P. E. M. *J. Organmet. Chem.* **1995**, *491*, 231.
(27) Sicilia, E.; Russo, N. *J. Am. Chem. Soc*. **2002**, *124*, 1471.
(28) Hall, C.; Perutz, R. N. *Chem. Rev.* **1996**, *96*, 3125.
(29) Wang, C. J.; Ye, S. *Int. J. Quantum Chem.* **1999**, *75*, 47.
(30) Russo, N.; Sicilia, E. *J. Am. Chem. Soc.* **2001**, *123*, 2588.
(31) Irigoras, A.; Elizalde, O.; Silanes, I.; Fowler, J. E.; Ugalde, J. M. *J. Am. Chem. Soc*. **2000**, *122*, 114.
(32) Irigoras, A.; Fowler, J. E.; Ugalde, J. M. *J. Am. Chem. Soc*. **1999**, *121*, 8549.
(33) Sudhakar, P. V.; Lammertsma, K. *J. Am. Chem. Soc*. **1991**, *113*, 5219.
(34) Sudhakar, P. V.; Lammertsma, K. *J. Org. Chem.* **1991**, *56*, 6067.
(35) Wang, Z.-X.; Liu, R.-Z.; Huang, M.-B. *Can. J. Chem.* **1996**, *74*, 910.
(36) Wang, Z.-X.; Huang, M.-B. *Can. J. Chem.* **1997**, *75*, 996.
(37) Wang, Z.-X.; Huang, M.-B. *J. Phys. Chem.* **1998**, *102*, 229.
(38) Wang, Z.-X.; Huang, M.-B. *J. Phys. Chem. A* **1999**, *103*, 265.
(39) Head-Gordon, M.; Pople, J. A.; Frisch, M. J. *Chem. Phys. Lett.* **1988**, *153*, 503.
(40) Beck, A. D. *J. Chem. Phys.* **1993**, *98*, 5648.
(41) Becke, A. D. *Phys. Rev. A* **1988**, *38*, 3098.
(42) Vosko, S. H.; Wilk, L.; Nusair, M. *Can. J. Phys*. **1980**, *58*, 1200.
(43) Lee, C.; Yang, W.; Parr, R. G. *Phys. Rev. B* **1988**, *37*, 785.
(44) Pople, J. A.; Krishman, R. *Int. J. Quantum Chem.* **1978**, *14*, 91.
(45) Gonzalez, C.; Schlegel, H. B. *J. Phys. Chem.* **1990**, *94*, 2154.
(46) Gonzalez, C.; Schlegel, H. B. *J. Phys. Chem.* **1990**, *94*, 5523.
(47) Hay, P. J.; Wadt, W. R. *J. Chem. Phys.* **1985**, *82*, 299.
(48) Frisch, M. J.; Trucks, G. W.; Schlegel, H. B.; Scuseria, G. E.; Robb, M. A.; Cheeseman, J. R.; Zakrzewski, V. G.; Montgomery, J. A., Jr.; Stratmann, R. E.; Burant, J. C.; Dapprich, S.; Millam, J. M.; Daniels, A. D.; Kudin, K. N.; Strain, M. C.; Farkas, O.; Tomasi, J.; Barone, V.; Cossi, M.; Cammi, R.; Mennucci, B.; Pomelli, C.; Adamo, C.; Clifford, S.; Ochterski, J.; Petersson, G. A.; Ayala, P. Y.; Cui, Q.; Morokuma, K.; Salvador, P.; Dannenberg, J. J.; Malick, D. K.; Rabuck, A. D.; Raghavachari, K.; Foresman, J. B.; Cioslowski, J.; Ortiz, J. V.; Baboul, A. G.; Stefanov, B. B.; Liu, G.; Liashenko, A.; Piskorz, P.; Komaromi, I.; Gomperts, R.; Martin, R. L.; Fox, D. J.; Keith, T.; Al-Laham, M. A.; Peng, C. Y.; Nanayakkara, A.; Challacombe, M.; Gill, P. M. W.; Johnson, B.; Chen, W.; Wong, M. W.; Andres, J. L.; Gonzalez, C.; Head-Gordon, M.; Replogle, E. S.; Pople, J. A. *Gaussian 98*, revision A.11; Gaussian, Inc.: Pittsburgh, PA, 2001.
(49) Collins, J. B.; Schleyer, P. v. R.; Binkley, J. S.; Pople, J. A. *J. Chem. Phys.* **1976**, *64*, 5142.
(50) Ehlers, A. W.; Bohme, M.; Dapprich, S.; Gobbi, A.; Hollwarth, A.; Jonas, V.; Kohler, K. F.; Stegmann, R.; Veldkamp, A.; Frenking, G. *Chem. Phys. Lett.* **1993**, *208*, 111.
(51) Chen, W.; Schlegel, H. B. *J. Chem. Phys.* **1994**, *101*, 5957.
(52) Wittbrodt, J. M.; Schlegel, H. B. *J. Chem. Phys.* **1996**, *105*, 6574.
(53) Goldstein, E.; Beno, B.; Houk, K. N. *J. Am. Chem. Soc.* **1996**, *118*, 6036.
(54) Boys, S. F.; Bernardi, F. *Mol. Phys.* **1970**, *19*, 553.